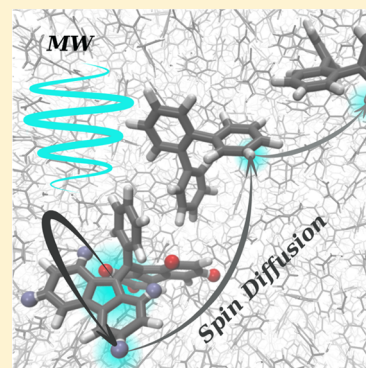


Molecular Mechanism of Overhauser Dynamic Nuclear Polarization in Insulating Solids

Svetlana Pylaeva,[†] Konstantin L. Ivanov,^{‡,§} Marc Baldus,[§] Daniel Sebastiani,[†] and Hossam Elgabarty^{*,†,§}[†]Chemistry Department, MLU Halle–Wittenberg, 06120 Halle (Saale), Germany[‡]International Tomography Center SB RAS, Novosibirsk 630090, Russia[§]Novosibirsk State University, Novosibirsk 630090, Russia[§]NMR Spectroscopy, Bijvoet Center for Biomolecular Research, Utrecht University, 3584 CH Utrecht, The Netherlands

ABSTRACT: Dynamic nuclear polarization (DNP), a technique that significantly enhances NMR signals, is experiencing a renaissance owing to enormous methodological developments. In the heart of DNP is a polarization transfer mechanism that endows nuclei with much larger electronic spin polarization. Polarization transfer via the Overhauser effect (OE) is traditionally known to be operative only in liquids and conducting solids. Very recently, surprisingly strong OE-DNP in insulating solids has been reported, with a DNP efficiency that increases with the magnetic field strength. Here we offer an explanation for these perplexing observations using a combination of molecular dynamics and spin dynamics simulations. Our approach elucidates the underlying molecular stochastic motion, provides cross-relaxation rates, explains the observed sign of the NMR enhancement, and estimates the role of nuclear spin diffusion. The presented theoretical description opens the door for rational design of novel polarizing agents for OE-DNP in insulating solids.



Dynamic nuclear polarization (DNP) is a powerful method to overcome one of the major drawbacks of NMR spectroscopy—its low sensitivity.^{1–6} At the core of any DNP technique is a mechanism that transfers the much higher electronic spin polarization to a nuclear spin, thus hyperpolarizing the latter. The resulting NMR enhancements can be very high, ideally reaching the value $\epsilon_{\max} = \gamma_e/\gamma_N$ equal to the ratio of the electronic and nuclear gyromagnetic ratios, which is about 660 for protons and even higher for other nuclei. Particularly in the past decade, DNP-based nuclear hyperpolarization has seen revolutionary advances, which have given rise to a number of new applications.⁷ This renaissance of the technique has naturally invoked intense efforts into the theory of DNP,^{8–16} with the general aim of improving the technique, designing more efficient polarizing agents, and extending its scope to higher magnetic fields and temperatures.

Solid-state DNP has mostly relied on either the solid-effect^{9,17} or the cross-effect^{10,18,19} as the hyperpolarization mechanism. Both effects are known to scale unfavorably with increasing strength of the external magnetic field and also to decrease upon increasing temperature, most likely due to the decrease in electronic relaxation times. DNP-NMR is usually performed at temperatures of around 100 K, although DNP measurements at lower temperatures (down to 10 K)^{20,21} and at high temperatures²² are also feasible.

Another polarization transfer mechanism, which is actually the only one operative in liquid-state DNP, is the Overhauser effect (OE).^{23–25} Although the possibility of OE-DNP in insulating solids was discussed very early by Abragam,²⁶ the mechanism was conventionally deemed important only in low-

viscosity liquids. However, recently, Can et al.²⁷ have reported OE-DNP effects operative in insulating solids. The authors have investigated DNP with both deuterated and protonated BDPA (Figure 1) (α,γ -bisdiphenylene- β -phenylallyl) radical

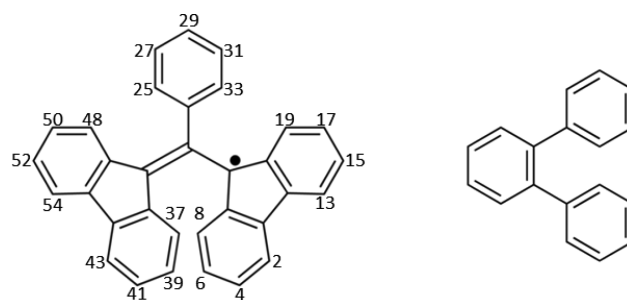


Figure 1. Structural formulas of the BDPA radical (left) and of OTP (right). Hydrogen atoms are omitted for clarity, and labels correspond to hydrogen atoms.

and the trityl OX063 radical embedded in a polystyrene matrix; the OE-DNP enhancement has been found only for BDPA and was shown to scale favorably with the magnetic field strength, that is, DNP enhancement increases in stronger magnetic fields. Lelli et al.²² further investigated this phenomenon for the BDPA radical in *ortho*-terphenyl (OTP, Figure 1) and

Received: March 7, 2017

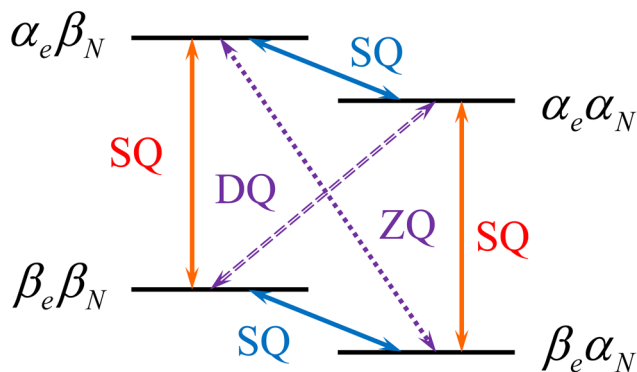
Accepted: April 26, 2017

Published: April 26, 2017

tetrachloroethane glassy matrix in a wide range of temperatures. Their findings revealed that a significant enhancement is preserved at temperatures as high as 240 K and that the enhancement is solvent-dependent. In fact, with OE enhancement, Lelli et al.²² obtained the largest DNP enhancement at high field (18.8 T) recorded to date.

The OE relies on a difference in rates of electron–nuclear zero-quantum (ZQ; flip–flop) and double-quantum (DQ; flop–flop) relaxation pathways (Scheme 1). Both types of

Scheme 1. Schematic Diagram of the OE in a Model System Comprised of an Electronic Spin Coupled to a Nuclear Spin^a



^aThe four-state spin system is represented as a direct product of the electronic and nuclear spin states: $\alpha_e \beta_e$, $\alpha_e \alpha_e$, $\beta_e \beta_e$, $\beta_e \alpha_e$. The four single-quantum (SQ) transitions are the allowed NMR and EPR transitions, while the ZQ and DQ cross-relaxation transitions are the ones responsible for OE.

cross-relaxation transitions are mediated by a fluctuating hyperfine interaction; the scalar hyperfine coupling (HFC) causes the ZQ transition (leading to a positive OE-DNP enhancement), whereas the dipolar HFC can cause both transitions (in the case of dipolar relaxation, the rates of the two transitions are different, usually leading to a negative OE-DNP enhancement). Thus, the relevant time correlation functions giving rise to the OE are those of the HFC

$$G_{l,m}(\tau) = \langle Y_{l,m}(t) Y_{l,m}^*(t + \tau) \rangle$$

$$J_{l,m}(\omega) = \int_{-\infty}^{+\infty} G_{l,m}(\tau) e^{i\omega\tau} d\tau$$

where the $Y_{l,m}$ are the spherical components of the HFC tensor, which is composed of a rank-zero part (the scalar coupling) and a rank-two part (the dipolar coupling).

For the fluctuations in the hyperfine tensor to be OE operative (i.e., to induce mutual relaxation transitions), they should exhibit time-dependent oscillations on a time scale comparable to $(\omega_e \pm \omega_N)^{-1} \approx \omega_e^{-1}$, where the ω 's are the Larmor frequencies of the electron and the hyperfine-coupled nucleus. The latter condition means that ideally the correlation time should be on the order of 10^{-11} to 10^{-12} seconds. In noninsulating solids, the conduction electrons provide the fast dynamics that facilitate OE. In insulating solids, however, molecular motion is almost never that fast and OE is usually deemed insignificant. To the best of our knowledge, the origin of the cross-relaxation mechanism responsible for the OE observed with BDPA in insulating solids remains unknown. Likewise, it is not clear which radical systems would provide

significant OE-DNP. The increased DNP enhancement upon increasing field has not been explained either. For all of these reasons, there is no rational strategy available for optimizing OE-DNP in solids to improve its performance.

Here, we present a theoretical investigation of OE-DNP in insulating solids. We have addressed this problem by a combination of computer simulation methods: classical and ab initio molecular dynamics (MD) simulations combined with spin dynamics (SD) simulations. Specifically, our aims were (1) to identify the molecular motion(s) responsible for the time dependence in the HFC and hence OE-DNP and (2) to pinpoint the particular structural properties of the BDPA radical that facilitate OE in contrast to other radicals where no effect was observed, for example, trityl radicals. As we demonstrate in this Letter, the origin of the observed OE-DNP lies in the low-frequency modes of BDPA and their couplings to the solvent bath. Specifically, these geometric fluctuations cause corresponding fluctuations in a spin density that is spread over a conjugated aromatic system. Importantly, such vibrational fluctuations are operative even in a solid matrix at low temperature, making solid-state OE-DNP feasible. SD simulations based on the spectral density extracted from MD trajectories show that the obtained estimates of the cross-relaxation rates are consistent, allowing us to simulate polarization of local nuclei as well as polarization of remote “bulk” nuclei, polarized by means of spin diffusion.

Altogether, we are able to model the phenomenon of OE-DNP in insulating solids using a joint approach combining molecular dynamics simulations with SD-based estimates of DNP enhancements. Analysis of the MD results paves the way to understanding which structural features to incorporate when designing new radicals suitable for OE-DNP in solids.

As already mentioned, in the heart of any OE-mediated DNP, there must be a fluctuation of the HFC with a correlation time on the order of the reciprocal of the electronic Larmor frequency. Moreover, the experimentally observed nuclear polarization requires a HFC that is not vanishingly small. MD-averaged proton HFC tensor components are presented in Table 1 for both cases: in vacuum (from ab initio MD) and in a frozen OTP glassy matrix (force field MD). We have partitioned the BDPA protons in six groups in a manner such as to maximize the correspondence with the six HFCs that were obtained from line shape simulations of the liquid-state

Table 1. MD-Averaged Proton HFC Tensor Components^a

group/ color	A, Exp. (MHz)	A, vacuum (MHz)	A, OTP (MHz)	D, vacuum (MHz)	D, OTP (MHz)	H number
A (red)	−5.54	−4.35	−4.49	0.84	1.06	4,8,15,19
B (blue)	−5.29	−4.17	−5.61	0.81	1.25	37,41,48,52
C	1.38	0.71	0.94	0.27	0.28	2,6,13,17
D	1.09	0.68	0.86	0.27	0.34	39,43,50,54
E	−0.5	0.33	0.88	0.42	0.50	25,29,33
F	−0.15	0.2	−0.12	0.14	0.17	27,31

^aVariables: A: isotropic coupling; D: one fifth of the Frobenius norm of the rank-two spherical tensor. Vacuum values were sampled from the an ab initio MD trajectory, while values from frozen OTP glass were obtained from the classical MD trajectory, as detailed in the Methods section. The A/B (red/blue) protons are marked in Figure 2a, and the proton positions are enumerated in Figure 1. Experimental values were taken from Can et al.²⁷

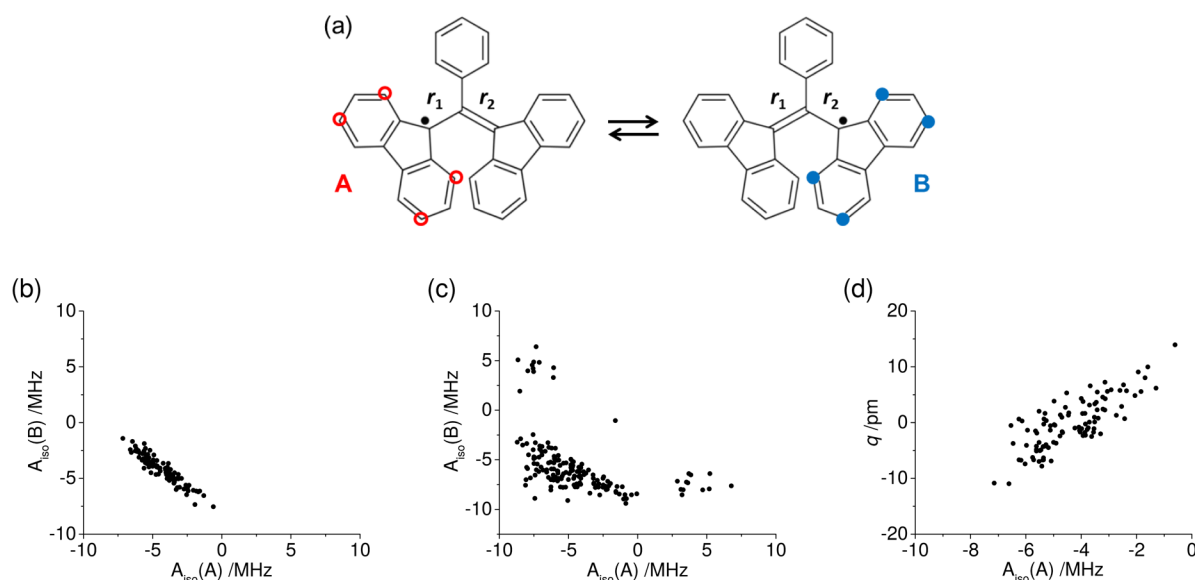


Figure 2. (a) Two *inequivalent* BDPA structures; only proton positions with the highest values of the isotropic HFC (corresponding to groups A and B in Table 1) are marked. (b,c) Interdependence of isotropic HFC constants of A and B groups in vacuum (b) and in the frozen OTP matrix (c). (d) Correlation between the reaction coordinate $q = r_1 - r_2$ and the isotropic HFCs of group A protons in vacuum.

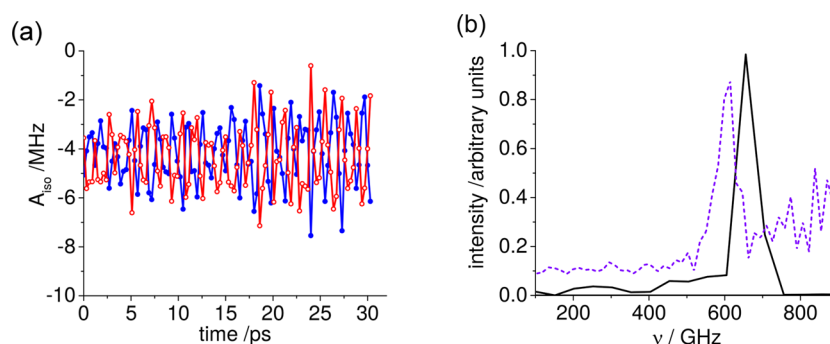


Figure 3. (a) Time evolution of the average isotropic HFC constants of the protons in groups A (red, open circles) and B (blue, solid circles) along the trajectory in vacuum (cf. Figure 2a). (b) Frequency spectrum of the asymmetry parameter $q = r_1 - r_2$ fluctuations. The black line is from the vacuum *ab initio* MD trajectory, and the purple dotted line is from the classical MD trajectory (frozen OTP matrix). Note that the dotted line is not shifted; the intensity in the range of 100–500 GHz depicts a broadened signal.

EPR spectrum of BDPA.²⁷ While this partitioning is not fully unambiguous, it provides good grounds for discussing the results, and as we will show later, it is consistent with the fluctuation patterns revealed by MD simulations.

By far, the strongest HFCs reside on the protons at the 1, 3, 6, and 8 positions of the fluorene moieties in BDPA (groups A/B in Table 1). These atoms are marked with red/blue in Figure 2a and occupy identical positions on the opposite fluorene groups. It is also clear from the table that in these two groups of protons the average of any component of the anisotropic HFC tensor is much weaker than the isotropic component. The time evolution of the average isotropic HFC of each of the two groups of protons in vacuum is depicted in Figure 3a. It is notable that the fluctuations exhibited by the scalar HFCs in each moiety are perfectly out of phase with those in the other one. Moreover, we found that in vacuum a negative linear correlation between couplings of both groups is very apparent (Figure 2b). In frozen OTP, the general correlation trend is preserved (Figure 2c), and expectedly, the correlation is noisier and exhibits some outliers with positive isotropic HFCs.

The out-of-phase fluctuations in the isotropic HFC constants imply an out-of-phase fluctuation in the spin density at these A/

B protons on the opposing fluorene moieties as well. Already, the periodicity of the fluctuations suggests an underlying vibrational mode in BDPA. Indeed, these spin density fluctuations can be best understood in terms of structural fluctuations between the two structures depicted in Figure 2a. This structural fluctuation can be captured in the dynamics of a single coordinate $q = r_1 - r_2$, where r_1 and r_2 are the bond lengths connecting the central carbon atom to the fluorene moieties. The fluctuations in q can be pictorially described as fluctuations between two alternating structures with a flipping in the bond orders. It should be noted that these two structures *are not* resonance structures as the geometry of BDPA is never planar. Plotting q against the scalar couplings of group A (or equivalently group B) protons indeed confirms the relationship (Figure 2d).

The large amplitude of the fluctuations in the HFC in response to small fluctuations in q (linear regression gives a slope of 0.12 MHz/pm) is a consequence of the delocalized electron density distribution at the two diphenylene moieties of BDPA and of the allylic bridge between them. Moreover, frequency analysis of the fluctuations of q in vacuum reveals that they are in the GHz range, with a maximal intensity at circa

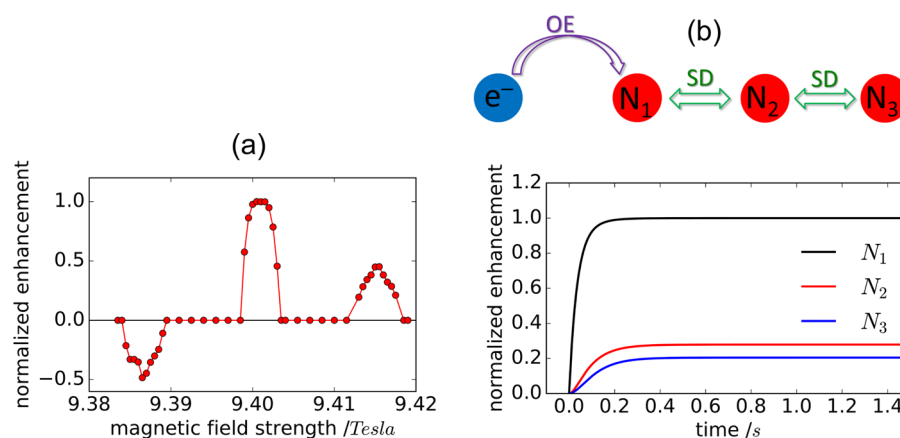


Figure 4. (a) Calculated magnetic field dependence of the DNP effect for $\omega_{\text{MW}} = 263.5$ GHz upon a sweep of the external magnetic field. The outer components in the “DNP spectrum” come from the solid-effect contribution, whereas the central component is due to OE-DNP. Parameters of the calculation are given in the [Methods](#) section. (b) Simulation of spin diffusion in OE-DNP; the time dependence of nuclear polarization of nuclei is shown. The spin system consists of one electron spin and three nuclear spins; OE-DNP is operative only for the N_1 nucleus nearest to the electron, whereas the N_2 and N_3 nuclei are polarized by spin diffusion. The field is tuned to the central component of the DNP spectrum. Other parameters of the calculation are given in the [Methods](#) section.

650 GHz (Figure 3b). In the frozen OTP matrix, the peak shifts to ~ 600 GHz, with the appearance of a nonvanishing spectral density in the 100–500 GHz range as well. Notably, ω_e falls into the same range: 140 GHz for 5 T, 263 GHz for 9.4 T, 395 GHz for 14.1 T, and 527 GHz for 18.8 T with the NMR spectrometer. Thus, our simulations reveal that there is indeed a sizable spectral density of the fluctuating HFC in the required range, facilitating DQ and ZQ cross-relaxation transitions. The vibrational nature of the oscillation in q means that it is active even at very low temperatures. Interestingly, fluctuations of the q peak at higher frequencies, which can offer an explanation for the experimentally observed increase in OE-DNP efficiency in this system at higher fields.²⁷ The stronger amplitude of the fluctuating scalar interactions (in contrast to dipolar couplings) also provides favorable conditions for OE-DNP at high fields because scalar HFC can only induce the ZQ relaxation process and not the SQ processes, that is, nuclear T_1 relaxation. An enhancement of the latter would reduce the resulting DNP efficiency. This is also in agreement with experimental findings, where a *positive* enhancement was found with protonated BDPA, but a *weaker and negative* enhancement was found in the case of deuterated BDPA.

For the simplest two-spin model depicted in Scheme 1 (one electron and one nucleus), we have used SD simulations to calculate the DNP efficiency for a field sweep around 9.4 GHz at a fixed MW frequency of 263.5 GHz. The resulting field dependence of the enhancement, that is, the “DNP spectrum”, exhibits three features (Figure 4a). The two outer features (a negative and a positive one) come from solid-effect DNP; these features emerge upon pumping the forbidden EPR transitions and are shifted by the nuclear Larmor frequency ω_N from the center of the spectrum. The feature in the center emerging upon pumping on EPR resonance comes from OE-DNP. This feature is positive as only the ZQ relaxation was taken into account (which is the case for fluctuating scalar HFC). The DNP spectrum pattern agrees with that reported earlier (e.g., Figure S1 in ref 22).

We have also simulated effects of spin diffusion. Such a consideration is critical as OE-DNP acts exclusively on local nuclei of BDPA, whereas only bulk nuclei can be observed in NMR experiments (and are in fact the intended target of the

enhancement). These distant nuclei are not coupled directly to the electron and thus can be polarized solely indirectly by polarization transfer from local nuclei, that is, by nuclear spin diffusion. To model spin diffusion, we have considered a system with three nuclei: one nucleus is coupled to the electron and is polarized directly, and the other two acquire polarization via dipole–dipole interactions. We located four spins on a chain and assumed that each spin is coupled to only its nearest neighbors, as depicted in Figure 4b. As expected, polarization of the local nucleus is the strongest at all times. However, other nuclei still acquire some nonthermal polarization by spin diffusion. Again, this is in agreement with the reported NMR experiments where sizable OE-DNP enhancements for bulk nuclei have been reported.²²

To summarize, we have revealed the molecular origin of the recently reported OE-DNP in insulating solids. Unlike liquid OE-DNP where fluctuations in the HFC are due to solvent dynamics, here the fluctuations have their origin in a superposition of local low-frequency modes in the radical itself and their coupling and broadening due to a solvent bath. These geometric fluctuations in turn cause corresponding fluctuations in the spin density at the radical’s protons. Both effects can be traced back to specific structural features: the two conjugated diphenylene moieties with their delocalized spin densities, the oscillating allylic bridge joining them, and of course the presence of structural protons in BDPA. The trytil radical, which failed to exhibit OE-DNP, has neither protons nor this strong dependence of the spin density on structural fluctuations. These findings already suggest a rationale for structural modifications that would render BDPA a more efficient DNP polarization agent. One approach would be to reduce the peak frequency of the structural fluctuations by increasing the masses of the fluorene moieties, for example, using massive substituents at the 2, 4, 5, or 7 positions of the fluorene (thus leaving intact the set of strong hyperfine-coupled protons). Electron-donating substituents could possibly offer an additional advantage by enhancing the spin density.

The conclusions based on this model and the ensuing spectral density are consistent with the reported experimental findings. The relative magnitudes of the scalar vs dipolar HFCs reveal that the former is dominant, as found experimentally.

The importance of structural protons in BDPA is also explained, and the frequency dependence of the OE-DNP density suggests a possible explanation for the OE-DNP field dependence. SD calculations predict sizable OE-DNP originating from ZQ cross-relaxation and estimate the role of nuclear spin diffusion from structural BDPA protons to bulk protons.

METHODS

Molecular Dynamics. Classical MD Simulations. Classical molecular dynamics simulations were performed using GROMACS 5.11²⁸ employing the Gromos53a6 force field.²⁹ Starting parameters for BDPA were downloaded from the ATB repository.³⁰ We reparametrized the stretching and torsional terms involving the central carbon by fitting to BLYP-D3 DFT calculations (setup described below). Simulations of a 32 mM solution of BDPA in OTP were done under the *NPT* ensemble in a cubic periodic box containing one molecule of BDPA. The system was simulated at room temperature (300 K) and pressure for 75 ns. Following this, the system was annealed down to 240 K over 1.1 ns, followed by 500 ps production for sampling the HFC tensors. Sequential snapshots were extracted from the production segment every 0.3 ps for calculation of HFC tensors.

Ab Initio Molecular Dynamics Simulations. A single BDPA molecule was simulated in a cubic periodic box with a side length of 27 Å, using the Gaussian-and-plane-waves method GPW³¹ and the BLYP-D3 density functional,^{32,33} a 400 Ry energy cutoff, combined with an accurate triple- ζ basis set with two sets of polarization functions,^{34,35} with a time step of 0.4 fs. All ab initio simulations were performed using CP2K.³⁶ The initial 6 ps were run under massive thermostating using the Nosé–Hoover³⁷ thermostat and a coupling time of 30 fs. The production part of the trajectory was run without thermostating (*NVE* ensemble) with a total length of 31 ps. Snapshots were extracted every 0.3 ps and used to calculate the HFC

Calculation of Hyperfine Coupling Tensors. Trajectory snapshots for calculating the HFC tensors were extracted regularly every 0.3 ps from the production segment of each trajectory (both the annealed classical trajectory and the ab initio trajectory). Calculations were performed in CP2K using the all-electron GAPW method,^{38,39} at a plane wave cutoff of 400 Ry, and the BLYP exchange correlation functional. A locally dense basis set was employed, with the EPR-III basis⁴⁰ for the hydrogen atoms and the Pople 6-31G* basis for carbon atoms.

Spin Dynamics. To gain insight into the mechanism of OE-DNP formation, we supported molecular dynamics by SD calculations. For these reasons, a program developed by some of us¹⁵ was modified for modeling DNP under magic angle spinning (MAS) conditions. We considered a spin system comprising an electron and up to three spin-1/2 nuclei. The Hamiltonian of such a system in the MW-rotating frame is as follows:

$$\hat{H}(t) = (\omega_e - \omega_{\text{MW}})\hat{S}_z + \omega_1\hat{S}_x - \omega_N \sum_k \hat{I}_{kz} + \sum_k \hat{\mathbf{S}}\hat{\mathbf{A}}_k\hat{\mathbf{I}}_k + \sum_{k < m} \hat{\mathbf{I}}_k\hat{\mathbf{D}}_{km}\hat{\mathbf{I}}_m \quad (1)$$

where ω_e is the Zeeman interaction of the electron spin, ω_{MW} is the MW frequency, ω_1 is the MW field strength, ω_N is the nuclear Zeeman interaction, $\hat{\mathbf{A}}_k$ is the hyperfine interaction tensor for the k th nucleus, and $\hat{\mathbf{D}}_{km}$ is the dipolar interaction

tensor for the k th and m th spins. As usual, $\hat{\mathbf{S}}$ and $\hat{\mathbf{I}}_k$ stand for the spin operators of the electron and nuclei. The Hamiltonian is time-dependent due to sample spinning and orientation-dependent ω_e , $\hat{\mathbf{A}}_k$, and $\hat{\mathbf{D}}_{km}$. Consequently, the MW pumping is not performed continuously on resonance but is rather occurring during “rotor events” at the instants of time when $\omega_e \approx \omega_{\text{MW}}$.²⁷ This leads to partial excitation of the EPR transition and to a shift of the electron spin magnetization away from equilibrium. Solid-effect DNP occurs at rotor events when $\omega_e \pm \omega_N \approx \omega_{\text{MW}}$ and forbidden EPR transitions are excited. Polarization transfer during rotor events is explicitly taken into account in our treatment. We considered polarization transfer between nuclei–spin diffusion, which is due to nuclear dipole–dipole interactions. Because relaxation effects are crucial for DNP formation, we took into account the electronic longitudinal and transverse relaxation (the corresponding relaxation times are denoted as T_{1e} and T_{2e}), cross-relaxation occurring at rates $1/T_{\text{ZQ}}$ and $1/T_{\text{DQ}}$ (for the ZQ and DQ transitions, respectively), and nuclear longitudinal relaxation with the time T_{1N} . The cross-relaxation rates were estimated from MD results as product $|\mathbf{A}|^2 J(\omega)$; here, \mathbf{A} is the matrix element of the fluctuating Hamiltonian for the corresponding transition and $J(\omega)$ is the spectral density at the transition frequency ω . In our SD calculations, we computed the evolution superoperator for the density matrix of the spin system, which describes the spin evolution over one MAS period, $T_{\text{MAS}} = 1/\nu_{\text{MAS}}$. After that, the density matrix was propagated over subsequent rotor periods until steady state was reached. We also performed averaging over different orientations of the radical with respect to the rotor-fixed frame.⁴¹ Typical parameters used in the simulation were as follows: MW frequency $\omega_{\text{MW}} = 2\pi \cdot 263.5$ GHz, MW field strength $\omega_1 = 2\pi \cdot 1$ MHz, isotropic g -factor 2.0026, g -anisotropy 0.005, isotropic HFC constant $A_{\text{iso}} = 2\pi \cdot 4$ MHz, dipolar HFC constant $A_{zz} = 2\pi \cdot 1$ MHz, and MAS frequency $\omega_{\text{MAS}} = 2\pi \cdot 10$ kHz. In all simulations, all nuclei were protons. Relaxation parameters were $T_{1e} = 10^{-3}$ s; $T_{2e} = 4 \times 10^{-6}$ s; $T_{1N} = 0.1$ s; $T_{2N} = 2 \times 10^{-4}$ s; $1/T_{\text{ZQ}} = 10$ s⁻¹; and $1/T_{\text{DQ}} = 0$. The estimate for T_{ZQ} follows the MD results; it has been taken to be equal to the product of $\langle A \rangle^2$ and the noise spectral density at the EPR frequency, $J(\omega_{\text{MW}})$. Here, $\langle A \rangle$ is the typical value of the scalar HFC of the red and blue groups of BDPA’s protons; see Table 1. To model spin diffusion, we assumed that the electron spin and nuclear spins are positioned on a line and set the distance between the nuclei equal to 3 Å, corresponding to a nuclear dipolar interaction of 4.4 kHz.

AUTHOR INFORMATION

Corresponding Author

*E-mail: hossam.elgabarty@chemie.uni-halle.de.

ORCID

Hossam Elgabarty: 0000-0002-4945-1481

Notes

The authors declare no competing financial interest.

ACKNOWLEDGMENTS

K.L.I. acknowledges support from the Russian Science Foundation (Grant No. 15-13-20035); S.P., H.E., and D.S. acknowledge support from DFG (Grant Se1008/12-1); and M.B. gratefully acknowledges financial support by an NWO VICI grant (Grant Number 700.100.443). The authors thank

Dr. Andrey Gurinov for support in running SD simulations and fruitful discussions.

REFERENCES

- (1) Maly, T.; Debelouchina, G. T.; Bajaj, V. S.; Hu, K.-N.; Joo, C.-G.; Mak-Jurkauskas, M. L.; Sirigiri, J. R.; van der Wel, P. C. A.; Herzfeld, J.; Temkin, R. J.; et al. Dynamic Nuclear Polarization at High Magnetic Fields. *J. Chem. Phys.* **2008**, *128*, 052211.
- (2) Griffin, R. G.; Prisner, T. F. High Field Dynamic Nuclear Polarization—the Renaissance. *Phys. Chem. Chem. Phys.* **2010**, *12*, 5737.
- (3) Ni, Q. Z.; Daviso, E.; Can, T. V.; Markhasin, E.; Jawla, S. K.; Swager, T. M.; Temkin, R. J.; Herzfeld, J.; Griffin, R. G. High Frequency Dynamic Nuclear Polarization. *Acc. Chem. Res.* **2013**, *46*, 1933–1941.
- (4) Ardenkjaer-Larsen, J. H.; Fridlund, B.; Gram, A.; Hansson, G.; Hansson, L.; Lerche, M. H.; Servin, R.; Thaning, M.; Golman, K. Increase in Signal-to-noise Ratio of > 10,000 Times in Liquid-state NMR. *Proc. Natl. Acad. Sci. U. S. A.* **2003**, *100*, 10158–10163.
- (5) Gajan, D.; Bornet, A.; Vuichoud, B.; Milani, J.; Melzi, R.; van Kalker, H. A.; Veyre, L.; Thieuleux, C.; Conley, M. P.; Grüning, W. R.; et al. Hybrid Polarizing Solids for Pure Hyperpolarized Liquids through Dissolution Dynamic Nuclear Polarization. *Proc. Natl. Acad. Sci. U. S. A.* **2014**, *111*, 14693–14697.
- (6) Chen, H. Y.; Ragavan, M.; Hilty, C. Protein Folding Studied by Dissolution Dynamic Nuclear Polarization. *Angew. Chem., Int. Ed.* **2013**, *52*, 9192–9195.
- (7) Jeschke, G.; Frydman, L. Nuclear Hyperpolarization Comes of Age. *J. Magn. Reson.* **2016**, *264*, 1–2.
- (8) Farrar, C. T.; Hall, D. A.; Gerfen, G. J.; Inati, S. J.; Griffin, R. G. Mechanism of Dynamic Nuclear Polarization in High Magnetic Fields. *J. Chem. Phys.* **2001**, *114*, 4922–4933.
- (9) Hovav, Y.; Feintuch, A.; Vega, S. Theoretical Aspects of Dynamic Nuclear Polarization in the Solid State - The Solid Effect. *J. Magn. Reson.* **2010**, *207*, 176–189.
- (10) Hovav, Y.; Feintuch, A.; Vega, S. Theoretical Aspects of Dynamic Nuclear Polarization in the Solid State - The Cross Effect. *J. Magn. Reson.* **2012**, *214*, 29–41.
- (11) Hu, K.-N.; Debelouchina, G. T.; Smith, A. A.; Griffin, R. G. Quantum Mechanical Theory of Dynamic Nuclear Polarization in Solid Dielectrics. *J. Chem. Phys.* **2011**, *134*, 125105.
- (12) Mentink-Vigier, F.; Akbey, Ü.; Hovav, Y.; Vega, S.; Oschkinat, H.; Feintuch, A. Fast Passage Dynamic Nuclear Polarization on Rotating Solids. *J. Magn. Reson.* **2012**, *224*, 13–21.
- (13) Thurber, K. R.; Tycko, R. Theory for Cross Effect Dynamic Nuclear Polarization under Magic-angle Spinning in Solid State Nuclear Magnetic Resonance: The Importance of Level Crossings. *J. Chem. Phys.* **2012**, *137*, 084508.
- (14) Thurber, K. R.; Tycko, R. On Mechanisms of Dynamic Nuclear Polarization in Solids. *Isr. J. Chem.* **2014**, *54*, 39–46.
- (15) Mance, D.; Gast, P.; Huber, M.; Baldus, M.; Ivanov, K. L. The Magnetic Field Dependence of Cross-effect Dynamic Nuclear Polarization under Magic Angle Spinning. *J. Chem. Phys.* **2015**, *142*, 234201.
- (16) Mentink-Vigier, F.; Akbey, Ü.; Oschkinat, H.; Vega, S.; Feintuch, A. Theoretical Aspects of Magic Angle Spinning - Dynamic Nuclear Polarization. *J. Magn. Reson.* **2015**, *258*, 102–120.
- (17) Jeffries, C. D. Polarization of Nuclei by Resonance Saturation in Paramagnetic Crystals. *Phys. Rev.* **1957**, *106*, 164–165.
- (18) Hwang, F.; Hill, D. A. Phenomenological Model for the New Effect in Dynamic Polarization. *Phys. Rev. Lett.* **1967**, *19*, 1011.
- (19) Hu, K.-N.; Yu, H.-h.; Swager, T. M.; Griffin, R. G. Dynamic Nuclear Polarization with Biradicals. *J. Am. Chem. Soc.* **2004**, *126*, 10844–10845.
- (20) Matsuki, Y.; Idehara, T.; Fukazawa, J.; Fujiwara, T. Advanced Instrumentation for DNP-enhanced MAS NMR for Higher Magnetic Fields and Lower Temperatures. *J. Magn. Reson.* **2016**, *264*, 107–115.
- (21) Bouleau, E.; Saint-Bonnet, P.; Mentink-Vigier, F.; Takahashi, H.; Jacquot, J.-F.; Bardet, M.; Aussenac, F.; Pura, A.; Engelke, F.; Hediger, S.; et al. Pushing NMR Sensitivity Limits Using Dynamic Nuclear Polarization with Closed-loop Cryogenic Helium Sample Spinning. *Chem. Sci.* **2015**, *6*, 6806–6812.
- (22) Lelli, M.; Chaudhari, S. R.; Gajan, D.; Casano, G.; Rossini, A. J.; Ouari, O.; Tordo, P.; Lesage, A.; Emsley, L. Solid-State Dynamic Nuclear Polarization at 9.4 and 18.8 T from 100 K to Room Temperature. *J. Am. Chem. Soc.* **2015**, *137*, 14558–14561.
- (23) Hauser, K.; Stehlik, D. *Advances in Magnetic Resonance*; Elsevier BV, 1968; Vol. 3; pp 79–139.
- (24) Loening, N. M.; Rosay, M.; Weis, V.; Griffin, R. G. Solution-State Dynamic Nuclear Polarization at High Magnetic Field. *J. Am. Chem. Soc.* **2002**, *124*, 8808–8809.
- (25) Griesinger, C.; Bennati, M.; Vieth, H.; Luchinat, C.; Parigi, G.; Höfer, P.; Engelke, F.; Glaser, S.; Denysenkov, V.; Prisner, T. Dynamic Nuclear Polarization at High Magnetic Fields in Liquids. *Prog. Nucl. Magn. Reson. Spectrosc.* **2012**, *64*, 4–28.
- (26) Abragam, A. Overhauser Effect in Nonmetals. *Phys. Rev.* **1955**, *98*, 1729–1735.
- (27) Can, T. V.; Caporini, M. A.; Mentink-Vigier, F.; Corzilius, B.; Walsh, J. J.; Rosay, M.; Maas, W. E.; Baldus, M.; Vega, S.; Swager, T. M.; et al. Overhauser Effects in Insulating Solids. *J. Chem. Phys.* **2014**, *141*, 064202.
- (28) Abraham, M. J.; Murtola, T.; Schulz, R.; Páll, S.; Smith, J. C.; Hess, B.; Lindahl, E. GROMACS: High Performance Molecular Simulations through Multi-level Parallelism from Laptops to Supercomputers. *SoftwareX* **2015**, *1–2*, 19–25.
- (29) Oostenbrink, C.; Villa, A.; Mark, A. E.; Van Gunsteren, W. F. A Biomolecular Force Field Based on the Free Enthalpy of Hydration and Solvation: The GROMOS Force-Field Parameter Sets 53A5 and 53A6. *J. Comput. Chem.* **2004**, *25*, 1656–1676.
- (30) Malde, A. K.; Zuo, L.; Breeze, M.; Stroet, M.; Poger, D.; Nair, P. C.; Oostenbrink, C.; Mark, A. E. An Automated Force Field Topology Builder (ATB) and Repository: Version 1.0. *J. Chem. Theory Comput.* **2011**, *7*, 4026–4037.
- (31) Lippert, G.; Hutter, J.; Parrinello, M. A hybrid Gaussian and Plane Wave Density Functional Scheme. *Mol. Phys.* **1997**, *92*, 477–488.
- (32) Grimme, S.; Antony, J.; Ehrlich, S.; Krieg, H. a Consistent and Accurate Ab Initio Parametrization of Density Functional Dispersion Correction (dft-d) for the 94 Elements H-Pu. *J. Chem. Phys.* **2010**, *132*, 154104.
- (33) Becke, A. D. Density-functional Exchange-energy Approximation with Correct Asymptotic Behavior. *Phys. Rev. A: At, Mol., Opt. Phys.* **1988**, *38*, 3098–3100.
- (34) Goedecker, S.; Teter, M.; Hutter, J. Separable Dual-space Gaussian Pseudopotentials. *Phys. Rev. B: Condens. Matter Mater. Phys.* **1996**, *54*, 1703–1710.
- (35) VandeVondele, J.; Hutter, J. Gaussian Basis Sets for Accurate Calculations on Molecular Systems in Gas and Condensed Phases. *J. Chem. Phys.* **2007**, *127*, 114105.
- (36) Hutter, J.; Iannuzzi, M.; Schiffmann, F.; VandeVondele, J. cp2k: Atomistic Simulations of Condensed Matter Systems. *WIREs Comput. Mol. Sci.* **2014**, *4*, 15–25.
- (37) Hoover, W. Canonical Dynamics: Equilibrium Phase-space Distributions. *Phys. Rev. A: At, Mol., Opt. Phys.* **1985**, *31*, 1695–1697.
- (38) Lippert, G.; Hutter, J.; Parrinello, M. The Gaussian and Augmented-plane-wave Density Functional Method for Ab Initio Molecular Dynamics Simulations. *Theor. Chem. Acc.* **1999**, *103*, 124–140.
- (39) Weber, V.; Iannuzzi, M.; Giani, S.; Hutter, J.; Declerck, R.; Waroquier, M. Magnetic Linear Response Properties Calculations with the Gaussian and Augmented-plane-wave Method. *J. Chem. Phys.* **2009**, *131*, 014106.
- (40) Barone, V. In *Recent Advances in Density Functional Methods (Part I)*; Chong, D. P., Ed.; Recent Advances in Computational Chemistry; World Scientific, 1995; pp 287–334.
- (41) Baldus, M. Correlation Experiments for Assignment and Structure Elucidation of Immobilized Polypeptides under Magic Angle Spinning. *Prog. Nucl. Magn. Reson. Spectrosc.* **2002**, *41*, 1–47.